Energy 140 (2017) 1252–1266

Contents lists available at ScienceDirect

Energy

journal homepage: www.elsevier.com/locate/energy

Design, modeling and experimental validation of a novel finned reciprocating compressor for Isothermal Compressed Air Energy Storage applications

Mahbod Heidari [a, *], Mehdi Mortazavi [b], Alfred Rufer [a]

[a] LEI, École Polytechnique Fédérale de Lausanne, Lausanne, Switzerland
[b] Department of Mechanical Engineering, Western New England University, 1215 Wilbraham Road, Springfield, MA, 01119, USA

ARTICLE INFO

Article history:
Received 7 March 2017
Received in revised form
4 September 2017
Accepted 7 September 2017
Available online 9 September 2017

Keywords:
Energy conversion and storage
Thermal
Pneumatic
Analogy
Transient heat transfer
Compressor
Experimental validation
Exergetic efficiency
Isothermal Compressed Air Energy Storage

ABSTRACT

Considering the need for a reliable and environmentally friendly energy storage solution for addressing renewable energy intermittency issue and following the developments on Isothermal Compressed Air Energy Storage (I-CAES) systems, a new finned piston compressor which is characterized by increased heat transfer area and coefficient has been designed, analyzed, manufactured and experimentally tested. This compressor includes two sets of concentric annular fins with different diameters: the mobile fins are pushed into the space between the stationary fins through a driver shaft and compress the air trapped in the interconnecting annular chambers while keeping the air temperature close to ambient. Modeling of heat transfer and fluid flow in such a complicated geometry with a transient, non-linear, multi-layer, multi-dimensional nature can be best done by equivalent electric analogies with variable resistances and capacitors and employing a lumped method. Using bond graph representation method and based on a previously developed model for a classic reciprocating compressor, energy conversion has been modeled using a conjugate heat transfer and fluid flow model. Results of the simulation are presented and have been validated using an experimental test bench and to provide contrast to current technology, compared to a classic reciprocating compressor. The heat transfer along one cycle has increased in the finned compressor by 32 times compared to a classic piston compressor. The results also reveal that however the volumetric efficiency is decreased slightly in the finned compressor (−8%), the exergetic efficiency has increased from 55.1% in a classic piston to 78.4% in the finned piston.

1. Introduction

Development of intermittent solar and wind energies and the demand peak increase has made energy storage very important in energy policy. Thus, energy storage will play a key role in enabling the world to develop a low-carbon electricity system [1].

Recently CAES has attracted attentions as a promising storage technology for medium term (daily) applications with high rated power and rated energy, long lifetime [2] and low levelized cost and greenhouse gas emission [3]. This concept is based on the natural compressibility of air. Thus, energy is stored in the form of pressure potential of compressed air.

In fact, CAES uses off-peak electricity to compress the air and stores it in a reservoir, either in an underground cavern or above-ground pipes or tanks. This energy can be utilized in the peak time using an expander coupled to an electric generator [4]. Traditional (Diabatic) CAES uses turbo machinery to compress air to around 70 bar before storage. In the absence of intercooling the air would heat up to around 900 K, making it impossible (or prohibitively expensive) to process and store the gas, however this way the heat of compression is wasted. To increase the output power, fuel is injected to the compressed air and ignited in a turbine [5]. Adiabatic CAES (A-CAES) stores the heat of compression and reuse it during the expansion, thereby removing the need to reheat with natural gas [6].This can be done in two ways: A-CAES without Thermal Energy Storage (TES) and A-CAES with TES. In A-CAES without TES, the heat of air is stored inside a combined thermal energy and compressed air storage volume, which restricts the storage pressure and consequently energy density, due to the high temperatures already achieved in rather low pressure ratios (e.g. 10 bar) [7].

* Corresponding author.
E-mail address: mahbod.heidari@epfl.ch (M. Heidari).

https://doi.org/10.1016/j.energy.2017.09.031
0360-5442/

Thus, this concept needs highly temperature resistant storage material, which implies high costs. To overcome this limitation, in A-CAES with TES, a dedicated TES device is used to store the heat of air separately, allowing the cooled pressurized air to be stored in any reservoir leading to higher storage pressure (at least 60 bar) and higher energy density [8,9].

Isothermal CAES (I-CAES) is an emerging technology, which attempts to overcome some of the limitations of traditional (diabatic or adiabatic) CAES. Rather than employing numerous stages to compress, cool, heat and expand the air, isothermal CAES technologies attempt to achieve true isothermal compression and expansion in situ, yielding improved round-trip efficiency and lower capital costs. In principle it also negates the need to store the heat of compression by some secondary means [10].

However, I-CAES is technologically challenging since it requires heat to be removed continuously from the air during the compression cycle and added continuously during expansion to maintain an isothermal process. Heat transfer occurs at a rate proportional to the temperature gradient multiplied by surface area of contact; therefore, to transfer heat at a high rate with a minimal temperature difference one requires a very large surface area of contact.

Although there are currently no commercial I-CAES implementations, several possible solutions have been proposed based upon reciprocating machinery. One method is using foam as a heat exchange interface [11]. The other method is to spray fine droplets of water inside the piston during compression. The high surface area of the water droplets coupled with the high heat capacity of water relative to air means that the temperature stays approximately constant within the piston – the water is removed and either discarded or stored and the cycle repeats. A similar process occurs during expansion [12]. While in previous works the sprayed water is atomized and heated up but not evaporated, as a more recent industrial application [13], utilizes sprayed water as two phase flow to facilitate heat exchange. Water injection is also proposed recently in a co-rotating scroll air compressor/expander to achieve isothermal process [14].

Another proposed I-CAES technology compresses and expands gas near-isothermally over a wide pressure range, namely from atmospheric pressure to about 200 bar. This large operating pressure range, along with the isothermal gas expansion (allowing for recovery of heat not achieved with adiabatic expansion), achieves a 7-fold reduction in storage cost as compared to classical CAES in vessels. The companies developing Isothermal CAES quote a potential round-trip efficiency of 70–80% [15].

As mentioned the objective of I-CAES is to keep the air almost at ambient temperature during both compression and expansion by increasing the heat transfer between air and solid surface of the compressor. One strategy to do so is to increase the heat exchange surface, by introducing a so-called *Directly Integrated Heat Exchangers* (DIHE) inside the compression/expansion chamber. A first solution realized using DIHE, was using a new concept of water-hydraulic gas compression/expansion. This concept uses columns of water as a "liquid piston" to compress the air while cooling and expanding it while heating it simultaneously [16], [17]. To further increase the surface area [18], has utilized liquid piston with porous media inserts for isothermal CAES applications leading to increase in efficiency and power density. Recently a liquid piston is also demonstrated in a test bench Ocean Compressed Air Energy Storage (OCAES) system [19].

However liquid piston shows promising results, requiring water as heat exchange medium, makes it technically challenging and complicated. In this paper another solution is proposed, which is to employ metal fins in a reciprocating piston compressor instead of water columns as DIHE. Thus, the subject of the current work is design, modelling and experimental validation of the proposed finned compressor. This paper is organised as follows:

In the second section, to gain a better understanding of the physics of the problem, thermodynamic principle of CASE is described. The proposed design and its components are described in section 3. The modelling methodology is not the focus of this study but is briefly introduced in section 4, adapted to a cylinder-piston assembly in section 5 and developed for the finned piston in section 6.

The input values for the numerical solution of the model is presented in section 7, and the results are shown in section 8 and validated using a dedicated test bench in section 9.

2. Physical principle of CAES

To show the advantage of isothermal CAES system over conventional CAES, it is interesting to study the physical principles and thermodynamics behind such systems. Fig. 1 shows the pressure-volume diagram of a CAES system. At point 1 the air from atmospheric pressure enters the compressor and at point 3 transfers to the reservoir at the final pressure. During the expansion phase, it enters an expander and reaches to point 1 again. Fig. 1(a) is a representation of a classic compression/expansion system. If we assume compression and expansion to be "quasi-static" processes, the area between the vertical axis and the compression curve (1-2-3) shows the work consumed by the compressor, while the area between the vertical axis and expansion curve (3-4-1) represents extractable work during expansion. Since the ratio of the extracted work is relatively negligible compared to work provided to the compressor, the overall round-trip efficiency is low. In Fig. 1(b) heat transfer enhancement has made it possible to save a part of the input work during compression, and to increase the work output during expansion. In Fig. 1(c) the idea is to perform both

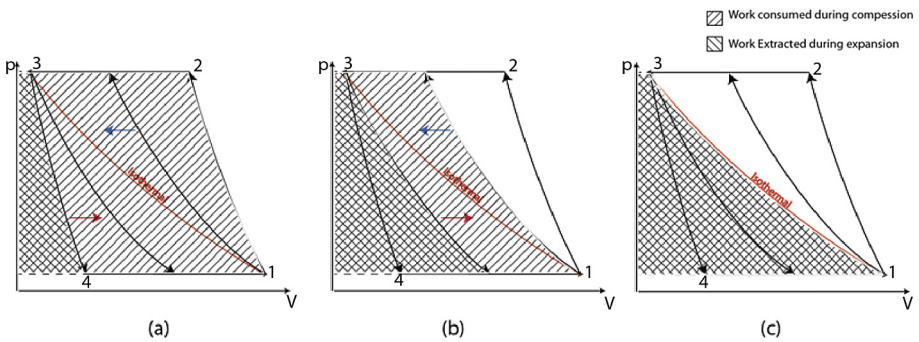

Fig. 1. Pressure-Volume Diagram during compression and expansion phase.

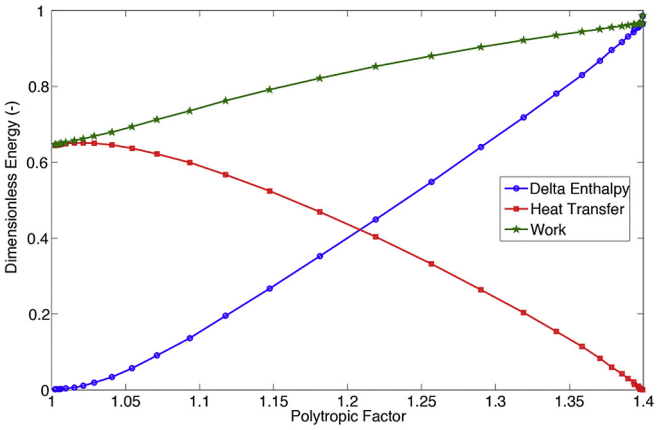

Fig. 2. Delta Enthalpy, heat transfer rate and work change with the polytropic factor.

compression and expansion as close as possible to isothermal process. In this way, the work of expansion will get closer to that of compression and the round-trip efficiency will approach unity.

Fig. 2 shows the effect of heat transfer on work input to a compressor. According to the first law of thermodynamics, the work input to a compressor may be written as:

$$\dot{W}_{in} = \dot{Q}_{out} + \Delta\dot{E} \quad (1)$$

Integrating over one cycle of a compressor cycle can calculate work input, heat transferred and difference of input and output enthalpy in the cylinder. If one changes the polytropic factor from 1.4 (adiabatic compression) to 1 (isothermal compression) the parameters in Eq. (1) will change according to Fig. 2 from right to left. It is observed that in the adiabatic case, however, the heat transfer is zero, but the delta enthalpy is at its maximum. By decreasing the polytropic factor heat transfer increases but the decrease in enthalpy difference is more significant, resulting in a reduction in total work. The same argument is true in an expander, which means maximizing the heat transfer (isothermal expansion) can maximize the output work.

3. Conceptual design of (dry) finned piston

To solve the problems associated with *liquid piston* technology [16] [17], such as solution of high-pressure air in liquid and the complexity of the design, a new concept has been proposed recently, called “dry (finned) piston” [20]. In this design, a series of concentric metal annuli's (sliding fins) which is attached to a linear guiding shaft, are fit into a fixed assembly of stator fins, to compress the trapped air. The stator and sliding fins are sized and spaced such that the sliding (piston) fins can fit in the spaces between adjacent stator (cylinder) fins, and the sliding fins fit in the spaces between adjacent stator fins so that the sliding fins nest and mesh with the stator fins.

The geometry of finned compressor is presented in Fig. 3. The precise linear movement of the shaft allows designing the system with a small gap between the adjacent fins. To minimize the dead volume, the gap between the fins is designed to be only 0.1 mm[1]. One should note the location of the seal in Fig. 3, and the fact that (at least a portion of) the air can circulate freely between the stator and sliding side chambers (There is no seal between the fins). In addition, the inlet/outlet of the finned compressor is designed

[1] The volume between the fins contributes only to 1% of the volume of cylinder (20% of the dead volume).

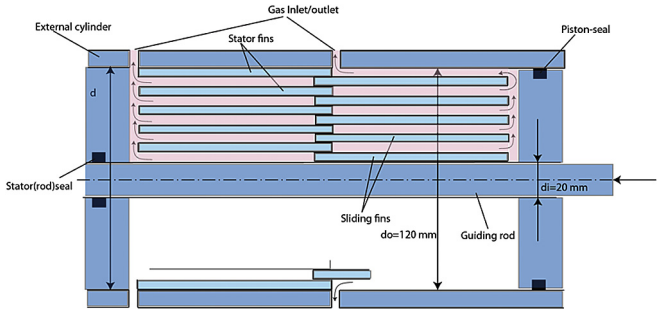

Fig. 3. Finned piston geometry.

through radial paths (on both sides), allowing the access to the internal layers.

Such a design, allows the heat exchange area to increases dramatically which increases the heat transfer leading to higher isothermal efficiency. This means that the extractable work increase during expansion while the consumed work decreases during compression. The resulting “quasi-isothermal” compression/expansion process leads to excellent roundtrip efficiency.

4. Principle of thermo-electric and pneumatic-electric analogies

Modelling heat transfer and fluid flow in the described finned compressor with complex geometry and transient operation is challenging, however it provides a great opportunity to employ and adapt appropriate modelling techniques to address an applied thermal engineering problem. This challenge is tackled by using transient Thermo-Electric Analogy Method (TEAM) and Pneumatic-Electric Analogy Method (PEAM). The principles of these methods are briefly described below.

4.1. Principle of thermo-electric analogy

In heat transfer, it is widely known that many textbooks [21,22], incorporate the electric circuit analogy. Historically, this analogy comes from the experimental works of Paschkis [23–25].

Educational publications [26] have used a similar approach but with emphasize on non-linear models for thermal conductivity and specific heat based on their dependency on temperature. More recently [27], have proposed an electrical software (SPICE) to model the multidimensional transient heat transfer.

In a similar approach with application to compressor technology [28], have used a *lumped capacitance method* to model the heat transfer in scroll compressors, considering a network of resistance and capacitance between different components of the compressor. However, accounting for time dependency of the equivalent circuit elements in such analogies is very rare. The novelty of this text is introducing resistance, capacitance and voltage sources that have variable values (throughout a cycle) as a function of time (e.g. when the geometry or heat transfer coefficients change over time) and applying this technique to a real industrial application.

There is a great interest in using a thermo-electric analogy with a lumped methodology for modeling the system containing several layers. The basic strategy of this methodology is to represent system elements (or zones) in as few thermal circuit elements as possible (lumping) when assembling thermal circuit of the system.

Thermal resistance network for combined series-parallel arrangement in steady state heat transfer is described in Ref. [21] as the addition of the total of the parallel resistance and the resistance in series (Fig. 4). This arrangement is similar to the

geometry of one of the chambers of the finned piston in steady states. This network can be further developed for an unsteady state condition where the boundary between parts *a* and *b* moves, or the compression of air generates heat and eventually the temperature of the walls increases over time which will be presented in the section 5.

4.2. Principle of pneumatic-electric analogy

Hydraulics analogy has been used widely to model and control hydraulic systems [29–33]. However, the analogy between pneumatic systems to electrical circuits with time-dependent values is rare in publications. This analogy is of great interest in systems with compressible - or incompressible - flow as working fluid and with time-dependent, high complexity and numerous similar or axisymmetric chambers, such as compressors and gas turbines. The finned compressor under study is interesting to be analyzed using such an analogy since it can be divided into similar subsystems.

It is common practice in hydraulics to choose pressure as effort (or potential) and volume flow as the flow variable. In pneumatics or gasses, however, since the density is not constant and the flow can be regarded as compressible, mass flow is considered as the flow variable.

Hagen-Poiseuille law indicates that pressure drop and mass flow rate are related as [22]:

$$\Delta p = \frac{128\mu l}{\rho\pi D^4}\dot{m} \tag{2}$$

Comparing (1) with Ohm's law indicates that resistance in pneumatic systems is proportional to the length of the channel and viscosity and is inversely proportional to the fourth power of diameter, and if the length of the channel or the viscosity of the gas changes over time, the resistance will be non-linear:

$$R = \frac{128\mu(t)l(t)}{\rho(t)\pi D^4} \tag{3}$$

Leakage of gas through seals can also be represented as a non-linear resistance. Assuming the leakage as an isentropic nozzle, the equivalent of this resistance can be represented as [34]:

$$R_{Leak} = \frac{1}{A_{Leak}p_u(t)}\sqrt{\frac{(k-1)R_gT_u(t)}{2k}} \tag{4}$$

where p_u and T_u are upstream temperature and pressure, and the leakage area (however very small) is the surface between the seals and the piston.

Ghafari et al. [35] have shown that the equivalent of the capacitor in pneumatic systems is proportional to the volume of the chamber containing the gas and is inversely proportional to polytropic index and temperature:

$$\mathrm{C} = \frac{\mathrm{V(t)}}{nR_gT(t)} \tag{5}$$

Since most of the real compressions are not isothermal, the capacitor will be non-linear.

It is possible to show that the equivalent of the inductor for a pipe with a cross section of A and length of *l*, which contains a gas with density of ρ, is [35]:

$$\mathrm{L} = \frac{\rho L}{A}l \tag{6}$$

But since the density of gasses is very low in comparison with liquids, we can often neglect the effect of inertia in pneumatics. The summary of the analogies used in this study is shown in Table 1. In this table, the bond graph representation is also included, where instantaneous power is transmitted between connected components by product of effort and flow.

5. Adaptation of TEAM and PEAM to cylinder-piston assembly

Modeling a reciprocating compressor deals with a series of complicated phenomena's occurring simultaneously in a relatively short period of time. Authors have shown the principles of reciprocating compressor modelling in Ref. [36] and in another article [37] that this can be best done by detaching pressure-mass flow as one pair (pneumatic bond) and temperature-heat transfer (thermal bond) and dealing with them separately. However, these parameter sets can't be fully detached since they are correlated by constitutive relations and energy and mass conservation equations, but by doing so the model can be handled easier. TEAM and PEAM will be applied to a simple piston compressor in section 5.1 and 5.2 respectively.

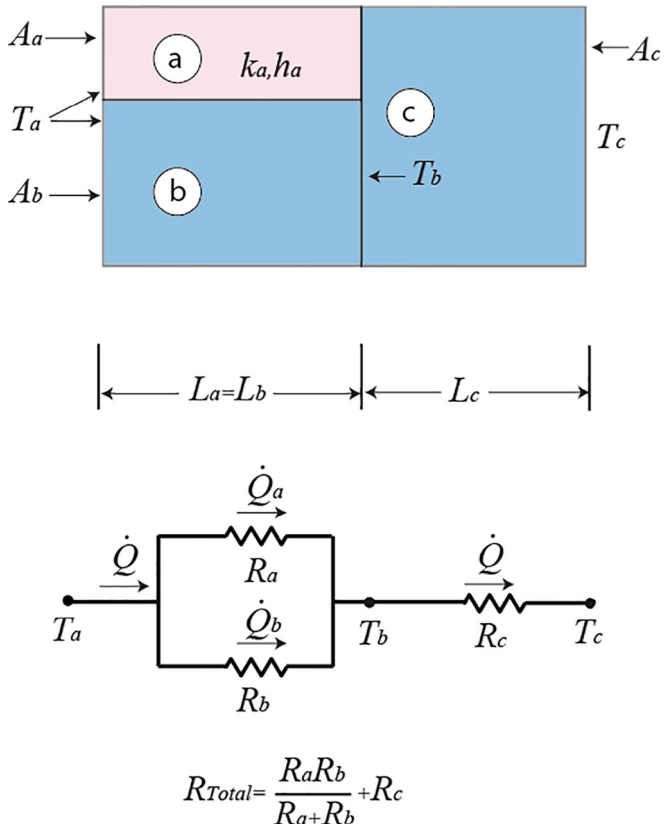

Fig. 4. Thermal resistance network for combined series-parallel arrangement [21].

Table 1
Equivalent variables in the pneumatic-electric analogy.

Case	Bond Graph	Flow	Effort	Capacitor	Resistor
Electrical	Φ / I	I	φ	C	R
Thermal	T / Q̇	Q̇	T	mc	$\frac{x}{kA(t)}$, $\frac{1}{h(t)A(t)}$
Pneumatic	P / ṁ	ṁ	p	$\frac{V(t)}{nR_gT(t)}$	$\frac{128\mu(t)l(t)}{\rho(t)\pi D^4}$

5.1. TEAM for simple cylinder-piston assembly

In section 4 it is assumed that the heat flow is uniform across the system that means no heat is being stored in the body of layers. However, in unsteady heat transfer analysis (which is the case for reciprocating compressors) this assumption is not always true since a part of the heat can be stored in the cylinder body. This will cause the introduction of a capacitor in the circuit. Consider a simple cylinder-piston assembly that its section is shown in Fig. 5. The cylinder-piston assembly is axisymmetric, and piston can move linearly upward and downward. While the piston compresses the gas, its temperature rises because the gas pressure increases. This acts as a heat generator, and since the temperature is being imposed by the cylinder head, it can be represented by a voltage source with a ground connection.

Fig. 6 shows the bond graph representation of the circuit in Fig. 5 where series elements (e.g. R_1, R_2) are represented by a (1) junction, while parallel elements (e.g. C_1) are shown by a (0) junction. *Se* (Source of effort) in both sides shows that the temperature is imposed (causally) from the left side by the cylinder head and from the right side by ambient.

The heat transfers to the first resistance R_1, being the sum of convection resistance (R_a) and half of conduction resistance (R_b) in the metal.

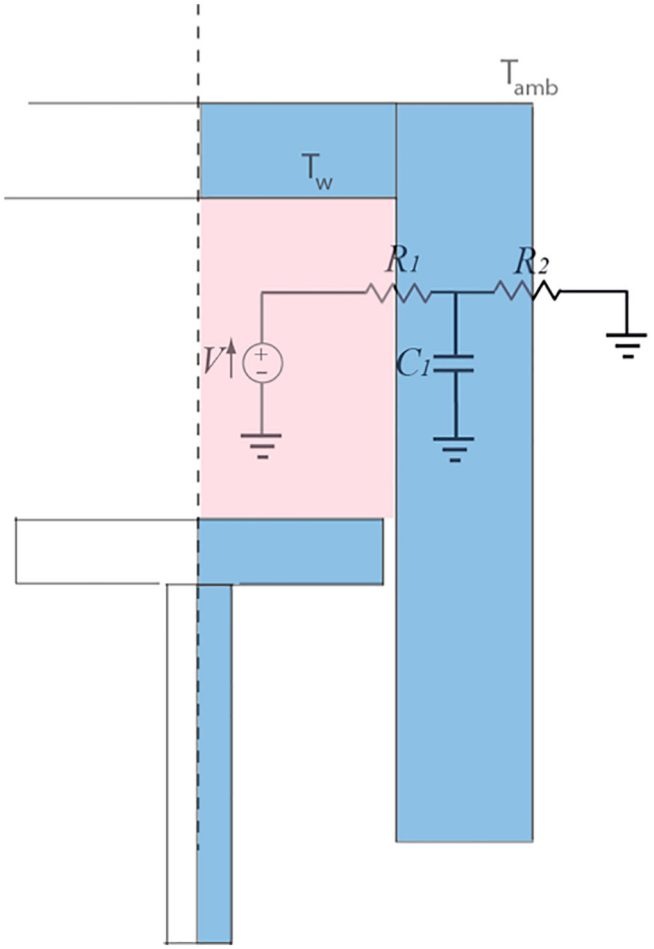

Fig. 5. Thermo-Electric analogy for a cylinder-piston assembly.

$$R_1(t) = R_a(t) + \frac{R_b}{2} \tag{7}$$

where

$$R_a(t) = R_{Conv}(t) = \frac{1}{h_1(t)A_i(t)} \tag{8}$$

In which A_i is the inner surface of compression chamber (which is variable and is a function of piston movement) and heat transfer coefficient (h_1) can be defined for air with conductivity coefficient k_a and diameter D_h, as:

$$h_1(t) = Nu(t)\frac{k_a}{D_h} \tag{9}$$

The Nusselt number is calculated using an approach to model the heat transfer in reciprocating compressors given by Eq. (10) developed by Adair [38].

$$Nu(t) = 0.053(Re(t))^{0.6}(Pr)^{0.8} \tag{10}$$

And for a metallic cylinder in cylindrical coordinates with inner diameter of D_1 and outer diameter of D_2 and conductivity k_b, thickness l,

$$R_b = R_{Cond,Metal} = \frac{\ln(D_2/D_1)}{2\pi lk} \tag{11}$$

So finally considering the gas temperature as $T(t)$.

$$\dot{Q}(t) = \frac{T(t) - T_w}{R_1(t)} \tag{12}$$

One should note that as Kirchhoff current law indicates a part of the convected heat ($\dot{Q}$) will be stored in the wall ($\dot{Q}_1$) while a part will be released to ambient ($\dot{Q}_2$).

$$\dot{Q}(t) = \dot{Q}_1(t) + \dot{Q}_2(t) \tag{13}$$

In the linear case, a thermal capacitance can be defined such that

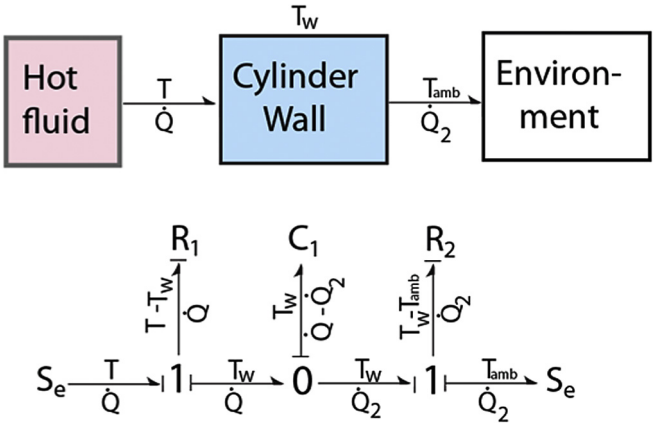

Fig. 6. Bond graph representation of the developed Thermo-Electric analogy.

$$T_w(t) = T_{w0} + \frac{1}{C1}\int_{t0}^{t} \dot{Q}_1(t)dt \tag{14}$$

where T_{w0} is the temperature at $t = t_0$. The capacitance C can be found by assuming that the cylinder body does negligible work by expanding or contracting, so the changes in its internal energy are only the result of $\dot{Q}_1$. Then if c is a *specific heat*,

$$c = \frac{\partial u}{\partial T} \tag{15}$$

where u is the internal energy per unit mass

$$C = mc \tag{16}$$

And m is the mass of cylinder body.

On the other hand, $\dot{Q}_2$ that is the heat transfers between the metal and outside ambient air is

$$\dot{Q}_2(t) = \frac{T_w(t) - T_{amb}}{R_2(t)} \tag{17}$$

where the second resistance R_2, is the sum of half of the conduction resistance (R_b) in the metal and convection resistance between wall and ambient (R_c)

$$R_2(t) = \frac{R_b}{2} + R_c(t) \tag{18}$$

and for the free convection from a cylinder, one can use the Rayleigh number computed approximately as

$$Ray(t) = \frac{gc_p}{T(t)\nu(t)^2\mu(t)k} D^3(T_w(t) - T_{amb}) \tag{19}$$

where g is the acceleration of gravity, T is the absolute temperature average of the surface of the cylinder and the environment (for an ideal gas only), ν is the associated specific volume, k is the thermal conductivity, D is the diameter, and $T_w(t) - T_{amb}$ is the temperature difference between the surface and the environment. For *Ray* in the usual wide range of 10^4 to 10^8 (for laminar flow), the Nusselt number is claimed by Ref. [39] to be well approximated by

$$\mathrm{Nu}(t) = 0.53Ray(t)^{0.25} \tag{20}$$

So the thermal resistance can be viewed as

$$R_c(t) = R_{Conv,amb}(t) = \frac{1}{\pi lkNu(t)} \tag{21}$$

At the end according to the first law of thermodynamics, the heat transfer rate that will be imposed to the cylinder head is

$$\dot{Q}(t) = p(t)\dot{V}(t) + \dot{E}_e(t) - \dot{E}_i(t) + \dot{U}(t) \tag{22}$$

Here $U(t)$ is the internal energy of the control volume, is assumed that the air obeys the gas law.

The values of R_a, R_b and R_c are shown in Fig. 7 for one cycles. Because the values of air velocity and the inside area of cylinder surface change alternatively over a cycle, R_a is variable. One may note that when piston reaches its TDC, the velocity of the piston (and hence *Re*) approaches zero, which increase the thermal resistance to a very high value. It is also observed that R_b value is very low compared to R_a and R_c. Also R_c can be decreased by applying a water jacket around the cylinder, so it is evident that the bottleneck in heat transfer enhancement is R_a.

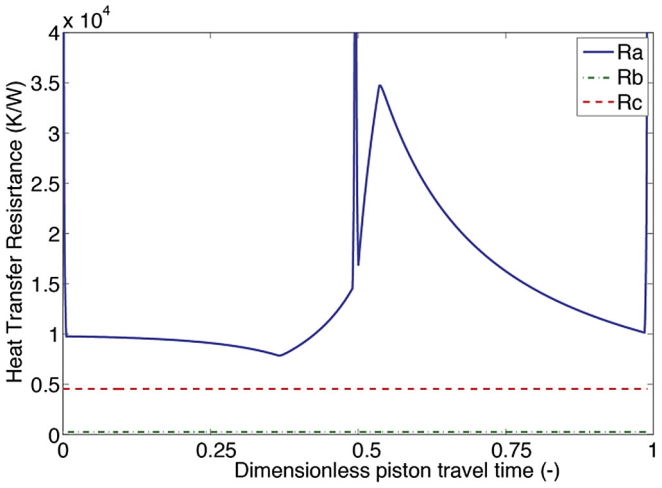

Fig. 7. Thermal resistance changes over a period of a cycle.

In section 6, it will be shown how the finned piston can overcome this problem.

The summary of the analogies used in this study is shown in Table 1.

5.2. PEAM for simple cylinder-piston assembly

The analogy described in the section 4.2 was first applied to a simple compressor model. Fig. 8 illustrates such an analogy. The shaft provides a force that is converted to the pressure change in the gas. This is shown by a voltage source in parallel with a variable capacitor with a ground connection. A variable volume chamber containing a compressible working fluid incurs a variable equivalent capacitance. Gas can move in and out of the cylinder through leakage or valve resistors. One should note that the leak resistance

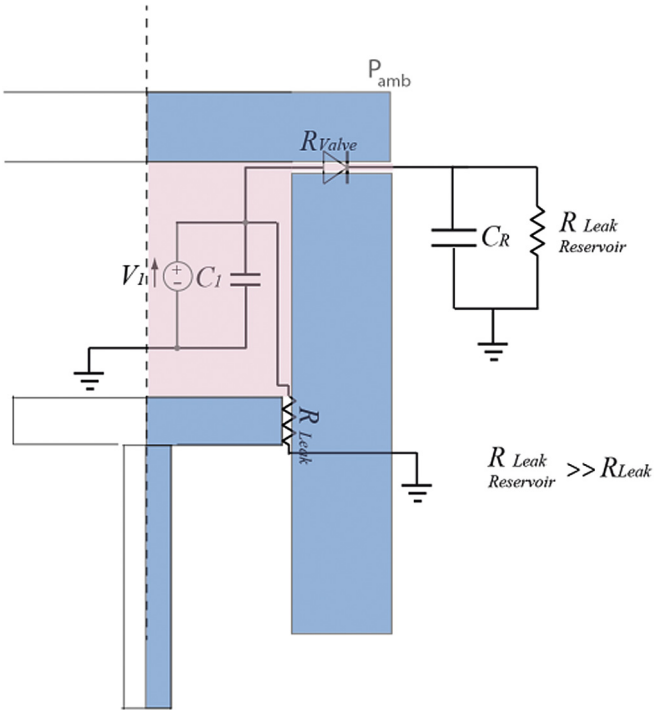

Fig. 8. Pneumatic-electric analogy for a classic cylinder-piston assembly.

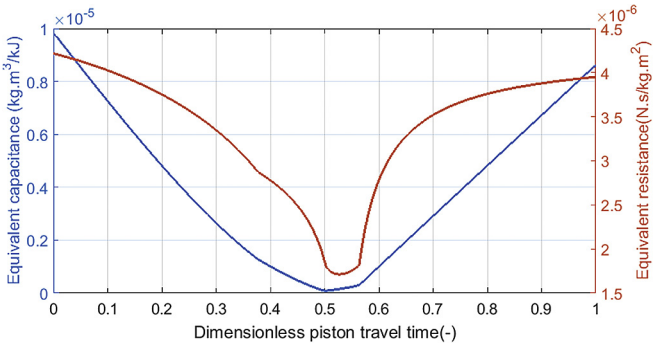

Fig. 9. Equivalent capacitance and leak resistance in pneumatic-electric analogy for variation over one cycle of the classic piston compressor.

in the reservoir is practically infinity and is placed for the sake of correctness of the electrical circuit. The leak resistance in the cylinder is due to the fact that seals are not perfect and there is always an amount of air leaking to outside, decreasing the volumetric efficiency but the amount of the leak resistance is much higher than the valve resistance. Since check valves allow the fluid to flow in one direction, it is more appropriate to model them as diode.

Fig. 9 illustrates the change of pneumatic capacity C_1 of cylinder and leakage resistance R_{Leak} as represented in Fig. 8 along one cycle. In the compression phase (0 < Dptt<0.5), the equivalent capacitance decreases as the volume of the chamber decreases and the temperature of gas increases. In expansion phase (0.5 < Dptt< 1), the equivalent capacitance increases as as the volume of the chamber increases and the temperature of gas decreases. The same trend is seen for leakage resistance: p_u and T_u (which are the gas pressure and temperature in compression phase) increase, however the effect of p_u is more dominant in Eq. (4) leading the resistance to decrease. The reverse happens in the expansion phase.

6. Development of the model for the finned piston

The low rate of heat transfer in classic cylinders motivated us to design a finned piston [20] in order to increase the overall heat transfer coefficient. The advantage of such a piston is that it increases both heat transfer coefficient h and heat transfer area A. By using a finned piston like the one in Fig. 3, the hydraulic diameter will be $D_o - D_i = 0.01$ m (Fig. 10(b)) instead of 0.120 m (Fig. 10 (a)) for a classic piston. Considering again Eq. (9), heat transfer coefficient is proportional to the inverse of D_h, so smaller hydraulic diameter means higher heat transfer coefficient. Also it is interesting to evaluate the heat transfer area increment in finned piston compared to a classic piston. Fig. 10 shows a classic as well as a finned piston at Bottom Dead Center (BDC), where piston is at its full expansion and Top Dead Center (TDC) where it is at its full compression. The finned compressor has the same stroke and clearance of the classic one. Fig. 11 shows the heat transfer rate and temperature of a classic compressor over one cycle. It is instructive to notice that in reciprocating compressor the highest potential of heat transfer is at TDC (because of high temperature difference), but the heat transfer area is very small since the piston is at its closest position to the cylinder head. The advantage of a finned piston is that the heat transfer area will remain constant and independent of the position of the piston, since there is a gap between fins and this allows the heat transfer to occur on the entire fins surface. Fig. 12 shows that the heat transfer area in the finned compressor is 5 times more at BDC and 18 times more at TDC compared to the classic compressor. As it will be seen later this along with higher heat transfer coefficient leads to a dramatic increase in heat transfer amount.

In the case of a finned piston, the Nusselt number for calculating the convection resistance (in Eq. (9)) was reported by Shah and London [40] for inside and outside annuli as

$$Nu_i = 7.54(D^*)^{-0.5}$$
$$Nu_o = 7.54(D^*)^{0.18} \quad (23)$$

where D^* is inner to outer annuli's diameter:

$$D^* = \frac{D_i}{D_o} \quad (24)$$

For finned piston (concentric annulus) the hydraulic diameter is equal to [22]:

$$D_h = D_o - D_i \quad (25)$$

In Fig. 13, the equivalent circuit is constructed for a single chamber of finned piston based on the same principles describe in section 5. In fact, air chambers (pink) can transfer the heat to their adjacent walls. As described in section 5, each resistant is the sum of the convection resistance and half of the conduction resistance of the adjacent wall. For example R_{11} is

$$R_{11} = R_{11a} + \frac{R_{11b}}{2} \quad (26)$$

Generally an indexed resistance R_{ij}, where i is the number of chamber or its corresponding vertical fin, shows the heat transfer resistance between:

R_{i1} : air chamber and inner adjacent annuli in the radial direction.
R_{i2} : air chamber and outer adjacent annuli in the radial direction.

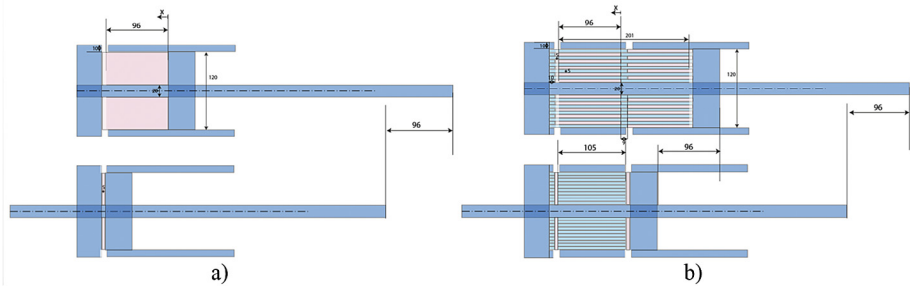

Fig. 10. Classic and finned piston positions at BDC and TDC.

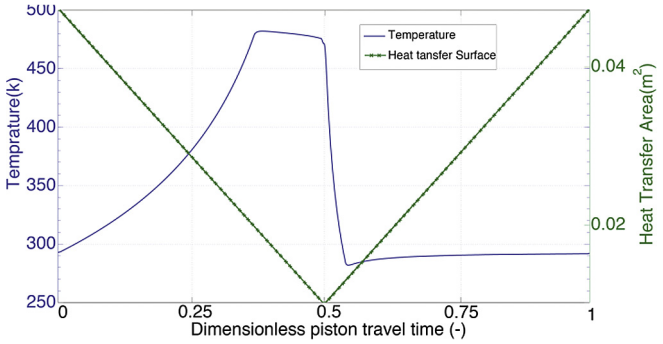

Fig. 11. Gas temperature and heat transfer area between gas to cylinder wall in the classic compressor.

R_{i3} : air chamber and its corresponding vertical fin in the axial direction.
R_{i4} : fin and upper cylinder wall in the axial direction.
R_{i5} : air chamber and inner adjacent annuli (within inter-fin space) in the radial direction.
R_{i6} : air chamber and outer adjacent annuli (within inter-fin space) in the radial direction.
R_{i7} : fin and lower cylinder wall in the axial direction.

The thermo-electric network for one chamber can be extended to the entire finned piston with four chambers as shown in Fig. 14 It is assumed that cylinder is axisymmetric around its axis. To account for the heat transfer in the axial direction a vertical network is implemented in the circuit. Vectorized code technique was used in programming to facilitate the computation of these values.

Authors have shown that such a model can be shown by a bond graph representation [41]. Such representation for the heat transfer part corresponding to TEAM is shown in Fig. 15.

The equivalent circuit for pneumatic-electric analogy can be found in Fig. 16. The upper chambers are connected by a small radial collecting channel that possesses resistance and capacitance effect at the same time $(R_{13}, C_{13}, \ldots)$. Also, the upper and lower chambers can exchange flow through the inner fin space (e.g., $R_{12}, R_{23}, \ldots$). There are also two leakage resistances since the finned piston has two seals.

Fig. 17 illustrates the change of pneumatic capacity (C_1) of the first chamber and pneumatic resistance between chamber 1 and 2 (R_{12}) that is represented in Fig. 16 along one cycle. Here the equivalent capacitance follows the same trend as in Fig. 9, however the volume of the chamber and also temperature change is smaller.

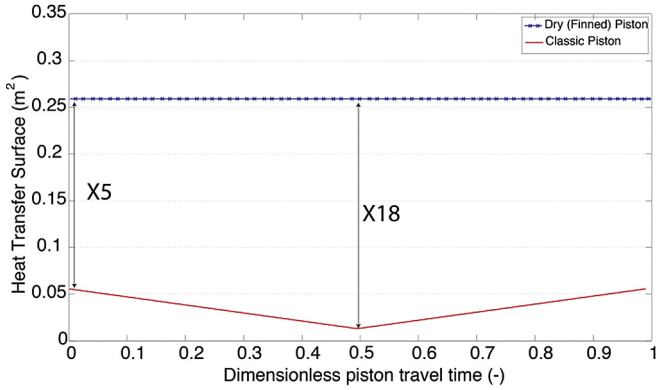

Fig. 12. Heat transfer area comparison along one cycle.

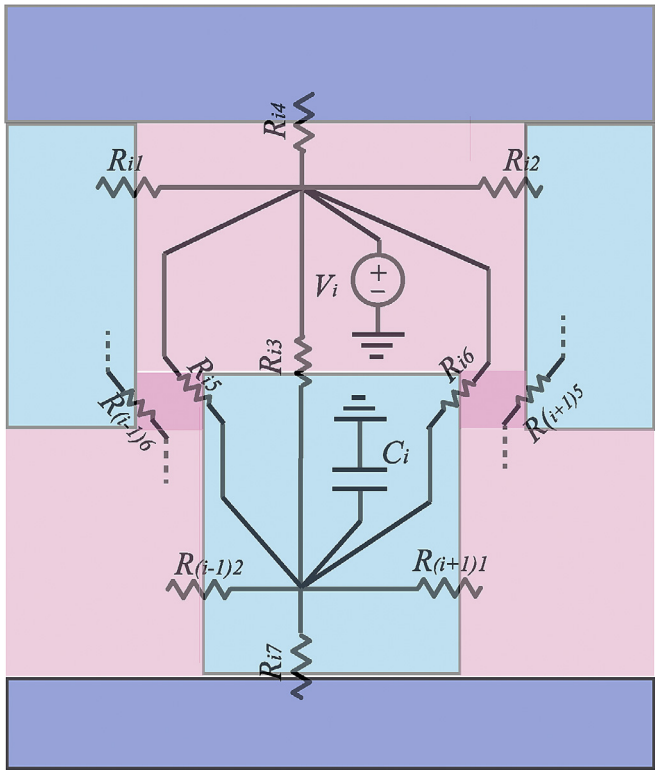

Fig. 13. Equivalent electrical circuit for the thermo-electric analogy for one chamber.

In compression phase, density and length of narrow channel between fins both increase, while the latter is more dominant in the first part and the former is more dominant in the second part of the compression.

The bond graph method can be employed to show the graphical representation of PEAM and is depicted in Fig. 18. The power transmitted to each of the chambers by the shaft work is shown in red, which corresponds to voltage generators in Fig. 16. This power is converted to pneumatic power while being stored in capacitors $(C_1, .., C_4)$ and flows between the chambers through the IFS resistances (R_{12}, R_{23}, R_{34}) and being distributed and collected through RCC resistances $(R_{13}, R_{24}, \ldots)$.

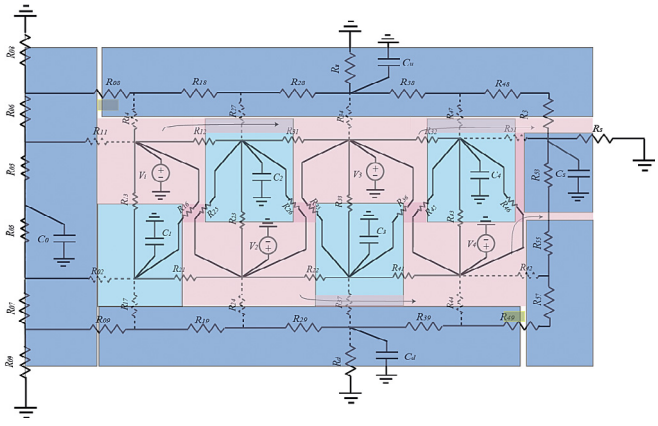

Fig. 14. Equivalent electrical circuit for the thermo-electric analogy expanded to the whole finned piston.

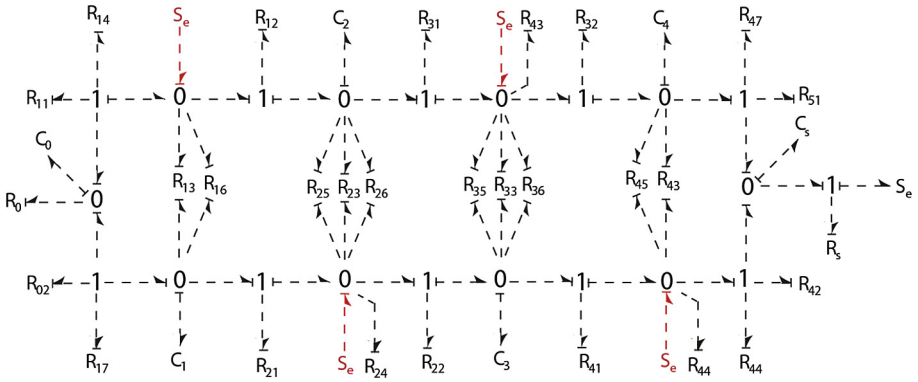

Fig. 15. Bond graph representation of the heat transfer in a finned compressor.

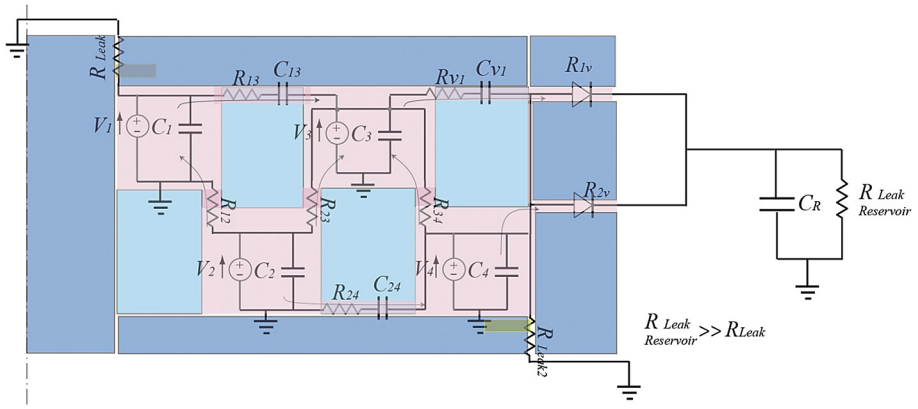

Fig. 16. Equivalent electrical circuit for the pneumatic-electric analogy.

7. Model inputs

In order to be able to compare the finned compressor to a classic one, the characteristics are designed to be equivalent. They both have a piston with an outer diameter of 12 cm and an inner diameter of 2 cm and a stroke of 96 cm and clearance of 5 cm. The period of a cycle is the same as before and equal to 1.98 s. The speed of the piston is constant during compression and expansion and is also equal to 100 $(mm\,s^{-1})$. The reservoir is the same as it was for the classic compressor, and initially at ambient temperature and pressure and its volume is 25 liters, which is again 20 times more than cylinder volume. Other inputs to the model required to estimate the gas compression effective work and efficiency for the classic and finned piston compressors using the equations developed are available as input variables are presented in Table 2.

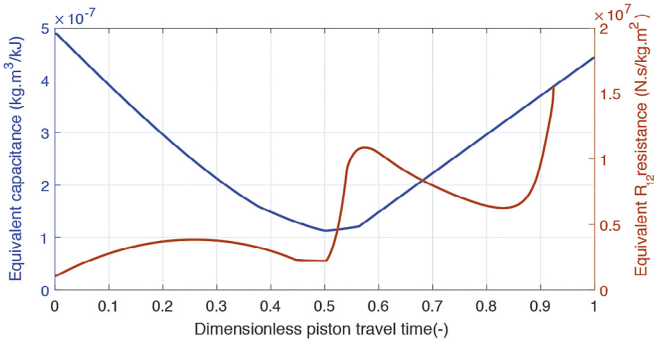

Fig. 17. Equivalent capacitance and resistance in pneumatic-electric analogy for variation over one cycle of finned compressor.

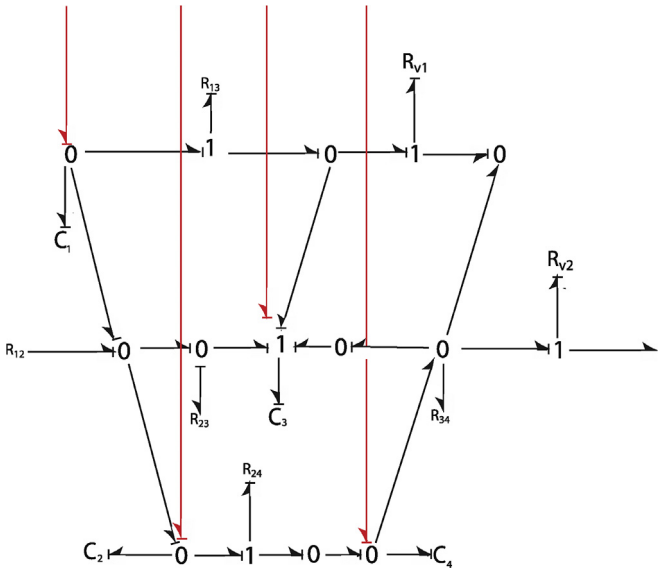

Fig. 18. Bond graph representation of the pneumatic part.

Table 2
Input variables for the numerical simulation of the classic and finned piston model.

Constant	Symbol	Finned compressor	Classic compressor	Units	Constant	Symbol	Finned compressor	Classic compressor	Units
Maximum cylinder volume	V_{max}	0.0011	0.0011	m^3	Reference dynamic viscosity	μ_0	$1.7*10^{-5}$	$1.7*10^{-5}$	$Pa.s$
Dead volume	V_0	0.000055	0.000055	m^3	Initial temperature	T_0	293	293	K
Piston stroke	l	0.96	0.96	m	Initial pressure	p_0	100	100	kPa
Piston clearance	x_0	0.005	0.005	m	Maximum pressure	p_{max}	580	580	kPa
Piston bore diameter	D_p	0.120	0.120	m	Inlet valve diameter	D_{vi}	0.006	0.006	m
Piston shaft diameter	D_0	0.02	0.02	m	Exit valve diameter	D_{ve}	0.006	0.006	m
Number of chambers	N	10	1	–	Gap between the fins	g	0.1	–	mm
Hydraulic diameter of main chambers	D_c	5	60	mm	Diameter of radial collecting channels	D_{rcc}	0.1	–	mm
Pressure compression ratio	p_r	5.8	5.8	–	Reservoir volume	V_{res}	0.025	0.025	m^3
Cycle period	T_{per}	1.98	1.98	s	Cylinder thickness	t_{cyl}	0.02	0.02	m
Piston linear speed	$\dot{x}_p$	0.1	0.1	m/s	Cylinder mass	m_{cyl}	9.5	4.5	kg

8. Results and discussion

First of all it should be noted that simulation and experimental validation has been carried out in two modes:

- *Fixed Pressure Mode* (FPM): In this mode the exhaust pressure is fixed at 580 *kPa* for the sake of simplicity in modelling and simulation over one cycle. All the results in the figures are related mode, unless stated otherwise.
- *Reservoir Filling Mode* (RFM): in this mode the exhaust is connected to a reservoir which is initially at ambient pressure and temperature. The reservoir is gradually filled with the compressed air after around 110 cycles (depending on HTC).

The differential equations involved in energy conversion of such a transient multi-dimensional, multi-layer system have time (t) as one independent variable in addition to cylindrical coordinates (r, x) and are very difficult (if not impossible) to solve analytically. The model for the entire finned piston was solved numerically using Matlab Simulink as the equation-solving program. In comparison to other methods (Finite difference, time and frequency domain method…), TEAM and PEAM methods simplifies (by lumping) the problem complexity at the model construction phase as opposed to computational phase. The resulting computations are simpler and therefore can be made with greater accuracy. Then results were compared to an equivalent classic piston. (The geometry of the both compressors are shown in Fig. 10). The classic piston model was developed earlier and verified using FEM and experimentation [36]. Also, a finite element model is developed for the finned piston to give more accurate results of local parameters as well as to provide a visual demonstration of the process [42]. Figs. 19 and 20 show some main thermodynamic parameters during one cycle in a fixed pressure level (FPL) mode. Fig. 19 shows the temperature of each chamber (from 1 to 4 as described in Fig. 16) was plotted along with the temperature of a classic piston. It is evident that the temperature in finned chambers rises much less (up to 320 K) than the classic piston (up to 480 K). The reason why the temperature of chamber 1 and 4 rises more is that they receive the inter heat transfer from one side while chambers 2 and 3 benefit from two sides. Also due to the higher heat transfer area in finned piston, the temperature of the gas decreases significantly during this exhaust stage, while the gas temperature in the reciprocating piston remains nearly constant.

Fig. 20 shows that the heat flux has been increased dramatically both in compression and expansion. The net heat transfer(which is the integral of heat flux curve) is 22 times more in compression and 45 times more in expansion for the finned piston(in average total heat transfer increases by a factor of 32 in the finned compressor). One may note that during the compression (first half of the cycle) the heat transfer is from gas to wall, while during expansion (second half of the cycle) it is from wall to gas.

The pressure evolution comparison between a classic piston compressor and each chamber of the finned piston compressor (from 1 to 4 as depicted in Fig. 16) is shown in Fig. 21 As it can be

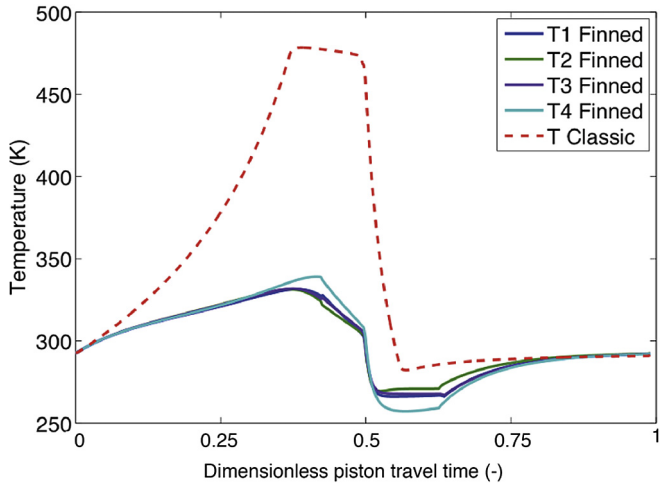

Fig. 19. Temperature evolution comparison.

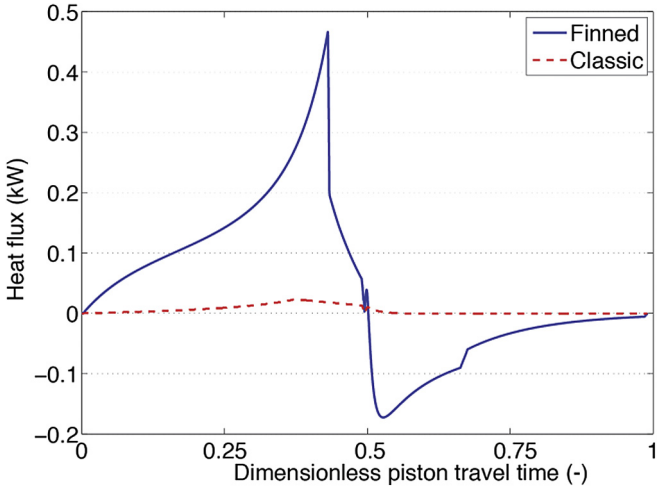

Fig. 20. Total heat flux comparison for one cycle.

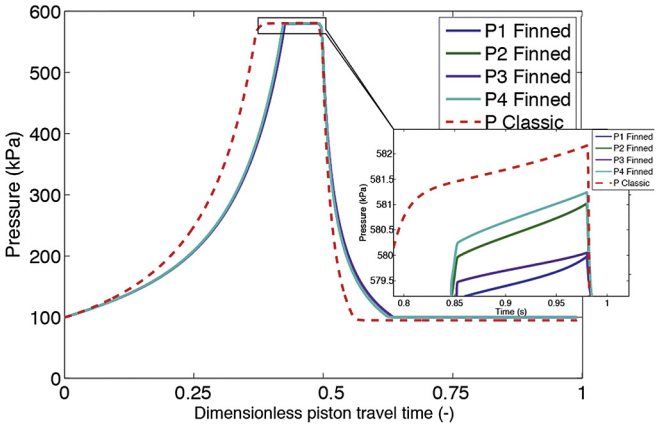

Fig. 21. Pressure evolution comparison.

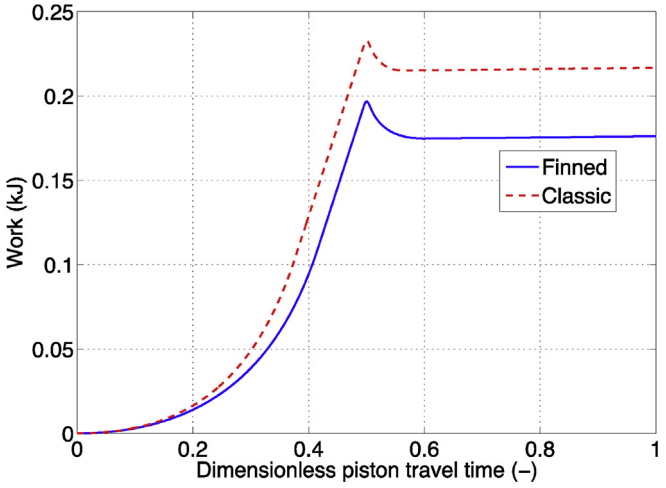

Fig. 22. Effective work comparison for one cycle.

seen, pressure evolution is less steep in the chambers of the finned piston (i.e. it takes longer time for the finned compressor to reach an exhaust pressure of 580 kPa) that means being closer to isothermal process. One may also note the pressure difference between upper and lower chambers of the finned compressor in the exhaust phase (in magnified zoom section) which induces flow between the chambers. As a result of the more isothermal process, the effective work has been decreased by 18% for the finned compressor in Fig. 22.

The results of the simulation for the finned compressor and its comparison to an equivalent classic compressor are summarized in Table 3. The effective work, which is the work required only for compressing the gas, is smaller for the finned piston, even though the friction work is greater, since the finned piston requires two seals. However, the total work (the sum of effective and friction work) is 16% lower for the finned compressor. One other important finding is that the discharged mass is slightly lower (9%) in the finned compressor as a result of lower volumetric efficiency, which is partly because of the more isothermal process[2] in the finned compressor. Finally, work per unit mass (which takes into account the effect of work and discharged mass together) is lower in finned piston compressor, which leads to higher isothermal and exergetic efficiencies.

9. Experimental validation

To validate the developed model of the complex thermodynamic processes, a test bench was developed to measure the power (which is the product of instantaneous force and velocity) and outlet pressure and temperature experimentally. The mobile and fix part of the finned piston are fabricated from exactly matching concentric annuli's with high precision from aluminum (Fig. 23), with the radial collecting channels that serve as inlet/outlet on the mobile part. The testbench includes a variable speed electrical motor to provide required work, a ball-screw driver for transforming rotational to linear movement, the classic or finned piston assembly, and apparatus needed for controlling speed and force, temperature and pressure sensors (Fig. 25). The schematic of the experimental setup is shown in Fig. 24. As seen, there are 2 check valves as inlet and 2 check valves as the outlet for finned compressor. Temperature and pressure sensors are located on the manifold that connects the outlets to the reservoir.

The velocity of the piston can be defined with very high precision and any desired profile. In this experiment a linear constant velocity of 100/mm/s) is used (Fig. 28)

As mentioned in RFM, the compressed air delivered by the finned compressor is stored in a reservoir, and as a result, the pressure level of the exhaust (and also of the reservoir) increases gradually from atmospheric to a given pressure level (580 kPa here).

The pressure and power raise evolution (during filling the reservoir) is shown in Figs. 26 and 27 For finned piston compressor, since the heat transfer coefficient relation (Eq. ((23)), has an uncertainty of ±20%, the curves of pressure raise have been plotted for these values as well. As expected, the model prediction of the pressure curves matches very well the experimental pressure, with the experimental pressure falling within the ±20% uncertainty error of heat transfer coefficient.[3]

For the finned piston compressor, the prediction of the model shows a reasonable match with experimental results, both in the way pressure and power raise as well as the shape of the power curve in any individual cycle.

The experimental force is compared to model prediction in Fig. 28 for the 100th cycle. In Fig. 29, the force is multiplied by velocity to product instantaneous power. The effect of uncertainty in heat transfer coefficient shown as it is seen for power rise. Experimental power falls within model prediction with ±20% heat transfer coefficient accuracy.

In the filling mode, The outer sleeve of finned compressor surface is measured with an infrared thermometer and compared to simulation in Fig. 30 and it agreed relatively well.

Since the operating speed is the only parameter that can be varied experimentally, a sensitivity analysis is conducted on it. This is accomplished by examining the sensitivity of the input work to change in compressor linear speed in filling mode. The test results were compared to the model prediction on a Parody diagram and it was found that the work input required to fill the reservoir up to 5.8 Bar matched the experimental results within 1% MAE with all points falling within ±2% of experimental results. The input work has a trend, which tends to under-predict the work at low speed and over predicts it in medium speed and again under predicts it in medium speed and again under predict it in higher speed (Fig. 31).

[2] In a more isothermal compression, the air trapped in the dead volume has lower temperature and higher mass compared to a less isothermal compression leading to reduced volumetric efficiency.

[3] The more isothermal process is, (which means higher heat transfer) the longer it will take to fill the reservoir with a given pressure level.

Table 3
Summary of the results of the numerical simulation of the finned piston and classic compressor models.

Term	Symbol	Classic compressor	Finned compressor	Units
Effective Work	W_{eff}	0.216	0.176	kJ/cyc
Friction Work	W_{frc}	0.038	0.04	kJ/cyc
Total Work	W_{tot}	0.255	0.215	kJ/cyc
Discharged mass	m_{disch}	$1.09*10^{-3}$	$0.98*10^{-3}$	kg/cyc
Work per unit mass delivered	w_{eff}	195.3	179.6	kJ/kg
Volumetric efficiency*	η_v	87.2	80.6	%
Isothermal efficiency*	η_{iso}	65.7	80.6	%
Exergy content of flow (After cool down)*	X_{acd}	0.11	0.124	kJ/cyc
Exergy efficiency*	$\eta_{ex,cs}$	50.9	70.4	%

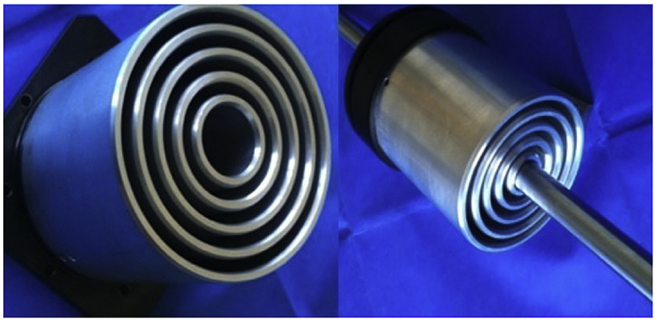

Fig. 23. Fix and mobile part of the finned piston-cylinder.

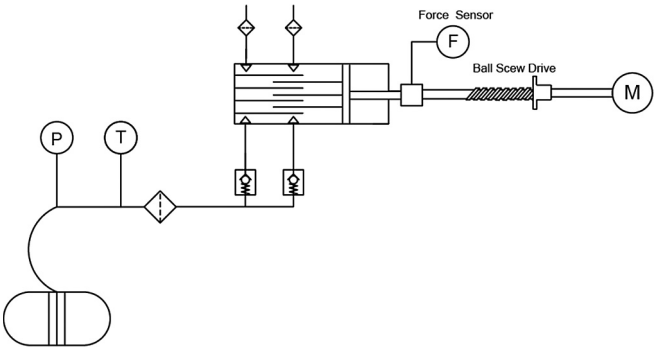

Fig. 24. Setup schematic circuit in filling mode.

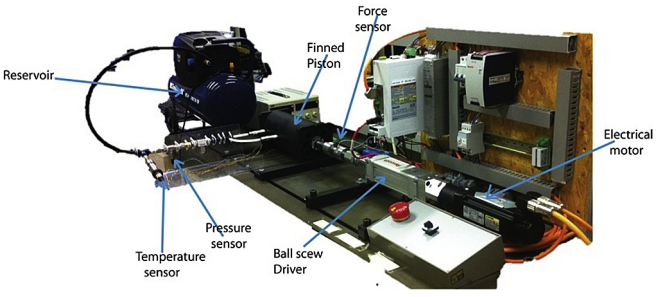

Fig. 25. Experimental setup.

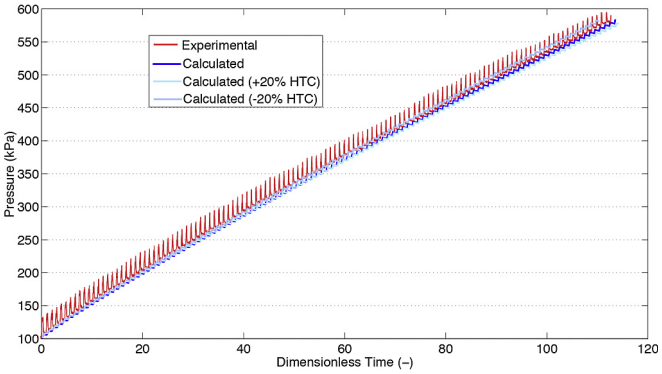

Fig. 26. Finned compressor simulated and experimental pressure comparison for RFM.

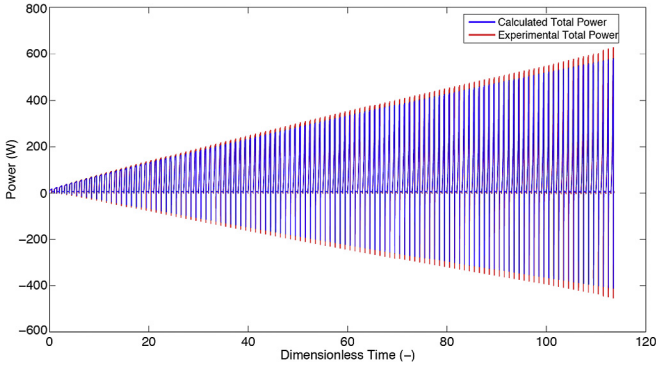

Fig. 27. Experimental and analytical power raise in finned piston compressor for RFM.

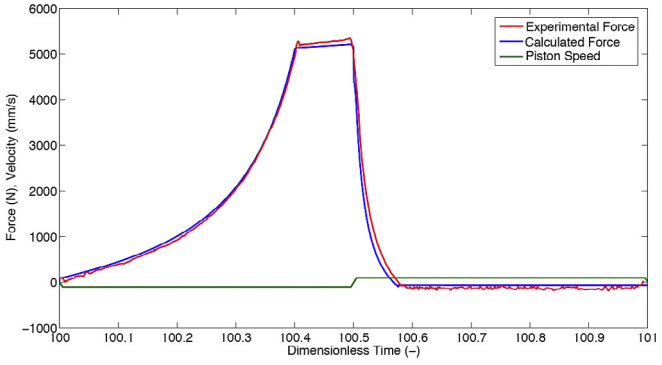

Fig. 28. Experimental and analytical force and velocity (100th cycle of RFM).

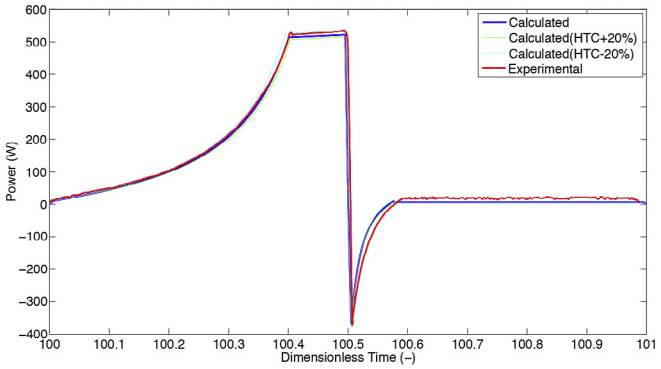

Fig. 29. Experimental and analytical power (100th cycle of RFM).

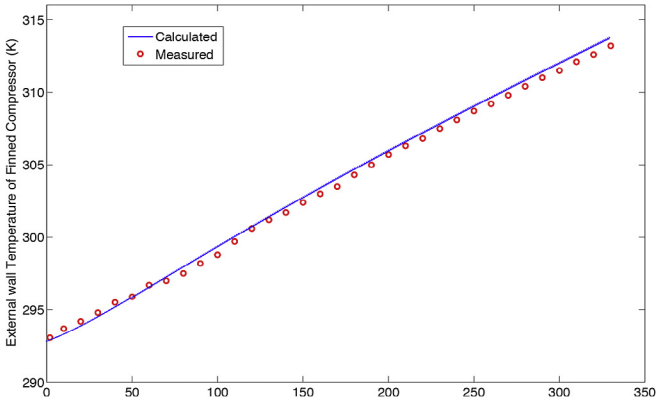

Fig. 30. Measured and calculated the temperature for finned compressor sleeve in RFM.

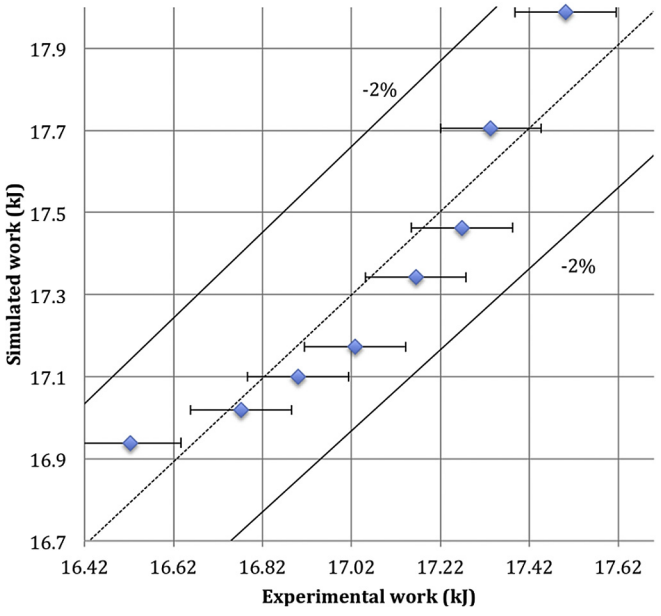

Fig. 31. Simulated compared against experimental work for finned piston compressor RFM (up to 580 kPa).

10. Conclusions

A new family of isothermal compressors, which are characterized by increased heat transfer area and low speed, has been designed for use in compressed air energy storage applications. In particular, the influence of the higher heat transfer area and coefficient at the end of compression phase (where the temperature reaches its peak) compared to classic compressors.

Regarding the design, rather than the flexible thermal elements found in the prior attempts to approach isothermal compression, the present design provides a fixed, rigid heat conductive fins within the chamber. The fins have a surface area which is large relative to that of the chamber itself. The present design provides a construction of a set of variable volume chambers that allows cycling of air to occur substantially isothermally, without the need for external heat exchangers. This results in smaller, simpler, cheaper, and more effective compressors.

The modelling process itself is carried out by the combination of a geometrical vectorized code for indexing the resistances and capacitors and thermo-electric and pneumatic-electricity analogy using a lumped method. This process has made the heat transfer and fluid flow modeling process of a complicated finned piston much easier. The resulting computations are simpler and take a shorter time.

In the new design, temperature rise during compression is decreased by 33% compared to a classic compressor. Meanwhile, in the finned compressor, the friction increases (+5%) and volumetric efficiency decreases (−8%) slightly compared to a classic compressor. however, the effect of reduced work is more dominant, resulting in a better exergetic efficiency (+30%) and reduced work required per unit mass (−8%) compared to a classic compressor.

This paper is a good example of how time-dependent electrical analogies can be used to model heat transfer and fluid flow in complicated energy conversion systems such as volumetric and turbomachines with complicated geometry. The same methodology is being used for modeling a scroll compressor as well as a liquid piston in an underway research. The methodology used in this study can have an impact on the future research in heat transfer modeling of energy systems with complicated geometries and transient nature.

List of abbreviations

BDC	Bottom Dead Center
CAES	Compressed Air Energy Storage
CV	Control Volume
DPTT	Dimensionless Piston Travel Time
FPM	Fixed Pressure Mode
FEM	Finite Element Method
HTC	Heat Transfer coefficient
IFS	Inter Fin Space
MAE	Mean Average Error
MCC	Main Compression Chambers
PR	Pressure Ratio
RCC	Radial Collecting Channels
RFM	Reservoir Filling Mode
RT	Round Trip
TDC	Top Dead Center

Nomenclature

U	Internal Energy (kJ)
Q	Heat Transfer (kJ)
$\dot{Q}$	Heat flux (kJ/s)

W	Work (kJ)
$\dot{W}$	Power (kJ/s)
E	Enthalpy (kJ)
$\dot{E}$	Enthalpy flow (kJ/s)
m	Mass (kg)
$\dot{m}$	Mass flow (kg/s)
V	Volume (m^3)
$\dot{V}$	Volume change (m^3/s)
T	Temperature (K)
p	Pressure (kPa)
ρ	Density (kg/m^3)
D	Diameter (m)
t	Time (s)
h	Heat transfer coefficient (W/m^2K)
Ray	Rayleigh number (−)
Re	Reynolds number (−)
Pr	Prandtl number (−)
μ	Dynamic viscosity (kg/m.s)
c_p	Specific heat at const. pressure (kJ/kg.K)
R_g	Gas constant (kJ/kg.K)
k	Heat conductivity (W/m.K)
A	Heat transfer Area (m^2)
φ	Electric potential (V)
I	Electric current (A)
R	Resistance (Ω)
C	Capacitance (F)
l	Length (m)
X	Position (m)
$\dot{X}$	Speed (m/s)
n	Polytropic exponent (−)
η	Efficiency

Subscript

a	air
b	body of metal
i	inlet
e	exhaust
p	piston
w	wall
h	hydraulic
u	upstream
v	valve
amb	ambient
acd	after cool down
$cond$	conduction
$conv$	convection
cs	compression and storage
atm	atmosphere
ex	exergetic
eff	effective
iso	isothermal

References

[1] Cavallo A. Controllable and affordable utility-scale electricity from intermittent wind resources and compressed air energy storage (CAES). Energy 2009;32:120–7.
[2] Energy Storage Association. [Online]. http://energystorage.org/.
[3] Abdon A, Zhang X, Parra D, Patel M, Baue K. Techno-economic and environmental assessment of stationary electricity storage technologies for different time scales. Energy 2017. https://doi.org/10.1016/j.energy.2017.07.097.
[4] Lund H, Salgi G. The role of compressed air energy storage (CAES) in future sustainable energy systems. Energy Convers Manag. 2009;50:1172–9.
[5] Succar S, Williams RH. Compressed air energy storage: theory, resources, and applications for wind power. 2008. Princeton, New Jersey, Technical report.
[6] Jakiel C, Zunft S, Nowi A. Adiabatic compressed air energy storage plants for efficient peak load power supply from wind energy: the European project AA-CAES. Int J Energy Technol Policy 2007;5:296–306.
[7] Mohamed EFA. Wind energy storage with uncooled compressed air. In: Electrical energy storage applications & technology conference (EESAT); 2003. San Francisco, California.
[8] Hobson MJ. Conceptual design and engineering studies of adiabatic compressed air energy storage (CAES) with thermal energy storage. No. PNL-4115. Pacific Northwest Lab., Richland, WA (USA). Columbia, MD: Acres American, Inc.; 1981.
[9] Barbour E, Mignard D, Ding Y, Li Y. Adiabatic compressed air energy storage with packed bed thermal energy storage. Appl energy 2015;155:804–15.
[10] Eckard R. CAES compressed air energy storage worldwide. 2010. Rockville, MD, USA.
[11] McBride T, Kepshire D. ICAES innovation: foam-based heat exchange. 2014. Seabrook, NH, USA.
[12] Coney MW, Stephenson PL, Malmgren A. Development of a reciprocating compressor using water injection to achieve quasi isothermal compression. In: International compressor engineering conference; 2002.
[13] Crane SE, Berlin Jr EP, Abkenar AP. Compressed air energy storage system utilizing two-phase flow to facilitate heat exchange. 2012. 8,215,105.
[14] Iglesias A, Favrat D. Innovative isothermal oil-free co-rotating scroll compressor–expander for energy storage with first expander tests. Energy Convers Manag 2014;85:565–72.
[15] Isothermal Compressed Air Energy Storage - SustainX. [Online]. http://www.sustainx.com/technology-isothermal-caes.htm.
[16] Lemofouet S, Rufer A. A hybrid energy storage system based on compressed air and supercapacitors with maximum efficincy point tracking. IEEE Trans. Indus. Electron Aug. 2006;53(no. 4).
[17] Lemofouet S, Rufer A. Investigation and optimisation of hybrid electricity storage systems based on compressed air and supercapacitors.: thèse EPFL, n° 3628. 2006.
[18] Yan B, Wieberdink J, Shirazi F, Perry Y. Experimental study of heat transfer enhancement in a liquid piston compressor/expander using porous media inserts. Appl Energy 2015;154:40–50.
[19] Park JK, Ro PI, He X, Mazzoleni A. Analysis, fabrication, and testing of a liquid piston compressor prototype for an ocean compressed air energy storage (OCAES) system. Mar Technol Soc J 2014;48(no. 6):86–97.
[20] M. Heidari and A. Rufer, "Analysis and development of a new compressor device based on the new finned piston," in 8th international conference on compressors and their systems, [London].
[21] Incropera F, Dewitt D. Fundamentals on Heat and Mass Transfer. New york: John Wiley andsons; 1996. p. 101–5.
[22] Çengel YA, Cimbala J. Essentials of fluid mechanics: fundamentals and applications. fifth ed. McGraw-Hill; 2008.
[23] Paschkis V. Electericalanalogy method for the investigation of transient heat flow problems. Ind Heat 1942;9:1162–70.
[24] Paschkis V, Baker A. Method for determining unsteady-state heat transfer by means of electrical analogy. Trans ASME 1942;64:105–12.
[25] Paschkis V, Heisler MP. The accuracy of lumping in an electric circuit, representing heat flow in cylindrical and spherical bodies. J Appl Phys 1946;17:246–54.
[26] Del Cerro F. The teaching of unsteady heat conduction using the thermo-electric analogy and the code pspice. Nonlineal models. In: International conference on engineering education and research "progress through partnership". VSB-TUO; 2004. Ostrava.
[27] Jena C, Sarbhai N, Mulaveesala R. Pulsed thermography simulation: 1D, 2D and 3D electro-thermal model based evaluation. In: In proc. National seminar on non-destructive evaluation; 2006.
[28] Chen Y, Halm N, Groll E, Braun J. A comprehensive model of scroll compressors, part II: overall scroll compressor modeling. In: In proceedings of the 2000 international compressor engineering conference at purdue; 2000. p. 725–34. West Lafayette, IN.
[29] Ljung L, Glad T. Modeling of dynamic systems. first ed. Prentice Hall; 1994. PTR.
[30] Love J. Process automation handbook: a guide to theory and practice. first ed. Springer; 2007.
[31] Macia NF, Thaler GJ. Modeling and Control of Dynamic Systems. first ed. Delmar Learn; 2004.
[32] Ogata K. Modern control engineering. third ed. Prentice Hall; 1997.
[33] Parr A. Hydraulics and pneumatics: a technicians and engineers guide. second ed. Butterworth-Heinemann; 1999.
[34] Karnopp DC, Rosenberg RC. System dynamics: modeling and simulation of mechatronic systems. 2000.
[35] Ghafari A, Maghsoudpour A, Pourmomtaz A. Control and dynamic systems. K.N.Toosi University Publications; 2006 (In Persian).
[36] Heidari M, Wasterlain S, Barrade P, Gallaire P, Rufer A. Energetic macroscopic Representation of A Linear reciprocating compressor model. Int J Refrig 2015. https://doi.org/10.1016/j.ijrefrig.2014.12.019.
[37] Heidari M, Rufer A. Bond graph model representation of a new reciprocating

finned air compressor. In: 11th international conference on bond graph modeling and simulation; 2014. Monterey, CA, USA.
[38] Adair RP. Instantaneous heat transfer to the cylinder wall in reciprocating compressors. In: Proc. Of the purdue compressor technology conf. IN, USA.: West Lafayette; 1972. p. 521–6.
[39] Holman JP. Heat transfer. seventh ed. McGraw-Hill; 1990.
[40] Shah RK, London AL. Laminar flow forced convection in ducts: a source book for compact heat exchanger analytical data/Publisher. New York: Academic Press; 1978.
[41] Heidari M, Rufer A, Thome JR. Thermoelectricity analogy method for computing transient heat transfer in a new reciprocating finned piston compressor. In: 15th international heat transfer conference; 2014. Kyoto, Japan.
[42] Heidari M, Barrade P, Rufer A. Modeling and simulation of a three-stage air compressor based on dry piston technology. In: COMSOL conference; 2011. Stuttgart, Germany.